

A conserved peptide-binding pocket in HyNaC/ASIC ion channels

Audrey Magdalena Ortega-Ramírez^a 📵, Simone Albani^{b.cd} 📵, Michèle Bachmann^a, Axel Schmidt^{a,1}, Manuela Pinoé-Schmidt^a, Marc Assmann^a, Katrin Augustinowski^a, Giulia Rossetti^{b,c,d}, and Stefan Gründer^{a,2}

Affiliations are included on p. 10.

Edited by Ehud Isacoff, University of California, Berkeley, CA; received May 7, 2024; accepted September 5, 2024

The only known peptide-gated ion channels—FaNaCs/WaNaCs and HyNaCs—belong to different clades of the DEG/ENaC family. FaNaCs are activated by the short neuropeptide FMRFamide, and HyNaCs by Hydra RFamides, which are not evolutionarily related to FMRFamide. The FMRFamide-binding site in FaNaCs was recently identified in a cleft atop the large extracellular domain. However, this cleft is not conserved in HyNaCs. Here, we combined molecular modeling and site-directed mutagenesis and identified a putative binding pocket for Hydra-RFamides in the extracellular domain of the heterotrimeric HyNaC2/3/5. This pocket localizes to only one of the three subunit interfaces, indicating that this trimeric ion channel binds a single peptide ligand. We engineered an unnatural amino acid at the putative binding pocket entrance, which allowed covalent tethering of Hydra RFamide to the channel, thereby trapping the channel in an open conformation. The identified pocket localizes to the same region as the acidic pocket of acid-sensing ion channels (ASICs), which binds peptide ligands. The pocket in HyNaCs is less acidic, and both electrostatic and hydrophobic interactions contribute to peptide binding. Collectively, our results reveal a conserved ligand-binding pocket in HyNaCs and ASICs and indicate independent evolution of peptide-binding cavities in the two subgroups of peptide-gated ion channels.

ligand-gated ion channel | molecular docking | neuropeptide | photo cross-linking | unnatural amino acids

DEG/ENaC ion channels have diverse functions. They comprise mechanosensitive ion channels, the degenerins (DEG) in Caenorhabditis elegans (1), constitutively open epithelial Na⁺ channels (ENaCs) in tetrapod vertebrates (2), and acid-sensing ion channels (ASICs) in diverse bilaterians (3). They also comprise the only known peptide-gated ion channels, which belong to two subgroups: FaNaCs and WaNaCs from different protostomes (4–6) and HyNaCs from the cnidarian Hydra magnipapillata (7, 8). Ion channels in both subgroups are activated by endogenous neuropeptides; FaNaCs/WaNaCs by RFamides and Wamides (4–6), respectively, and HyNaCs by Hydra RFamide I and Hydra RFamide II (in the following RFamide I and RFamide II, for brevity) (7, 8). Notably, FaNaCs/WaNaCs and HyNaCs are not closely related but have separated early in evolution. Whereas FaNaCs/WaNaCs are more closely related to degenerins and ENaCs and belong to clade B DEG/ENaCs, HyNaCs are more closely related to ASICs and belong to clade A DEG/ ENaCs (9, 10). In addition, RFamides from protostomes, such as FMRFamide, are evolutionarily unrelated to Hydra RFamides (11), suggesting that FaNaCs/WaNaCs and HyNaCs evolved independently. Determining whether the ligand-binding sites and gating mechanisms in these two subgroups are related or not would shed further light on the evolution of ligand binding in this ion channel family.

Despite their diverse functions, DEG/ENaCs share a similar trimeric structure, where each of the protomers has two transmembrane domains and a large extracellular domain (ECD) in between; the intracellular N and C termini are comparatively short. Based on the crystal structure of chicken ASIC1, the ECD of ASICs has been compared to a clenched hand with a palm domain from which the thumb, finger, and knuckle domains extend; the palm, thumb, and finger domains surround the central β-ball domain (12). FaNaCs have two sequence insertions in their ECDs that are not present in ASICs and HyNaCs: insertion I between $\alpha 4$ and $\alpha 5$ at the top of the thumb domain and insertion II between $\alpha 6$ and $\alpha 7$ of the knuckle domain (13). The knuckle and finger domains are at the tip of the ECD, and the finger domain has been implicated in ligand binding of FaNaCs by several studies (13–16). The cryo-EM structures of Aplysia californica and Malacoceros fuliginosus FaNaCs have recently confirmed that FMRFamides bind to a cleft located at the top of each protomer, which is formed by the finger domain and the knuckle domain from a neighboring subunit, and which is far away from the membrane (~70 Å) (17, 18). No such cleft is present in ASICs (17, 18). Ligand recognition in

Significance

Rapid transmission between neurons is mediated by ligandgated ion channels (LGICs). Most LGICs are activated by small-molecule neurotransmitters. The only known LGICS that are activated by neuropeptides belong to the DEG/ENaC ion channel family and belong to two groups—FaNaCs/WaNaCs and HyNaCs. In our study, we identified the single peptidebinding pocket in HyNaCs, showing that it is different from the peptide-binding pocket of FaNaCs/WaNaCs. This result indicates that peptide-activated LGICs evolved independently at least twice during the evolution of nervous systems. However, the peptide-binding pocket of HyNaCs is conserved in related acidsensing ion channels, mammalian ion channels that are activated by protons, identifying a conserved ligand-binding pocket in a subclass of DEG/ENaCs.

Author contributions: A.M.O.-R., M.B., A.S., G.R., and S.G. designed research; A.M.O.-R., S.A., M.B., A.S., M.P.-S., M.A., and K.A. performed research; A.M.O.-R., S.A., M.B., A.S., G.R., and S.G. analyzed data; and S.G. wrote the

The authors declare no competing interest.

This article is a PNAS Direct Submission.

Copyright © 2024 the Author(s). Published by PNAS. This article is distributed under Creative Commons Attribution-NonCommercial-NoDerivatives License 4.0

¹Present address: Institute of Human Genetics, University of Bonn, School of Medicine & University Hospital Bonn, Bonn 53127, Germany.

²To whom correspondence may be addressed. Email: sgruender@ukaachen.de.

This article contains supporting information online at https://www.pnas.org/lookup/suppl/doi:10.1073/pnas. 2409097121/-/DCSupplemental.

Published October 4, 2024.

FaNaCs appears to be primarily based on hydrophobic interactions (17, 18).

In contrast to FaNaCs, the secondary structure of HyNaCs aligns well with that of ASICs with only one longer deletion between $\alpha 1$ and $\alpha 3$ of the finger domain (8). Therefore, it is conceivable that HyNaCs have an overall structure similar to that of ASICs and do not possess a ligand-binding cleft at the top of the ECD, like FaNaCs. This raises the question of where ligands bind in HyNaCs. ASICs have a highly negatively charged cavity, the acidic pocket, which is formed by intrasubunit contacts between the thumb, the β -ball, and the finger domains, together with intersubunit contacts to the palm domain of an adjacent subunit (12). The acidic pocket has been proposed as the pH sensor of ASICs (12). Although functional studies indicate that the acidic pocket cannot be the sole pH sensor in ASICs (19-23), structural studies show that it collapses during protonation, which may open the ion pore (12, 24). Moreover, the peptide toxin PcTx1 and the opioid neuropeptide big dynorphin (Big Dyn) bind to the acidic pocket (25-28) to modulate ASIC gating (29, 30). Thus, although the acidic residues of this pocket are not conserved in HyNaCs, this cavity remains a candidate ligand-binding site in HyNaCs.

FaNaCs are homotrimers with three identical ligand-binding sites (17, 18), whereas HyNaCs are obligate heteromers (8, 31). In *Xenopus* oocytes, 10 different HyNaC subunits assemble into 13 different heteromeric ion channels. HyNaC2 is an obligate subunit that assembles with one subunit from subgroup 1 (HyNaC5, HyNaC6, or HyNaC7) and another subunit from subgroup 2 (HyNaC3, HyNaC4, HyNaC8, HyNaC9, HyNaC10, or HyNaC11) to form functional peptide-gated channels (8). This complex arrangement suggests that the individual subunits have different functions and make different contributions to ligand recognition.

Here, using HyNaC2/3/5 and a combination of molecular modeling, site-directed mutagenesis, and photo cross-linking using unnatural amino acids, we provide compelling evidence that HyNaCs have a single peptide-binding cavity at a subunit interface in the ECD at a position that corresponds to the acidic pocket of ASICs. Thus, our results show that peptide binding evolved independently in FaNaCs/WaNaCs and HyNaCs and identify a conserved ligand-binding cavity in HyNaCs and ASICs.

Results

HyNaC2/3/5 has a 2-5-3 Arrangement of Subunits. We used the HyNaC2/3/5 heteromer (31) as a model to study the ligand-binding site of HyNaCs. Because subunit interfaces are different in a trimeric complex wherein subunits are arranged clockwise in a 2-3-5 or a 2-5-3 order when viewed from the top, we first determined the order of the subunits in the heteromeric complex. Inspection of homology models of the 2-3-5 and 2-5-3 complexes, which were based on the resting conformation of chicken ASIC1 (cASIC1; PDB ID 6AVE) (24), identified two residues in HyNaC3 (N213 and F330) that are located at subunit interfaces on the two opposite sides of the protomer in both models (Fig. 1A). We substituted these two amino acids individually with the unnatural amino acid azido-phenylalanine (azF), which allows the cross-linking of these residues by UV irradiation to other amino acids around them. Both mutant channels were functional (SI Appendix, Fig. S1) and were tagged with a C-terminal HA epitope. When we coexpressed HA-tagged HyNaC3 carrying the azF substitution at position 213 or 330 together with HyNaC2 and HyNaC5 in HEK293 cells and subjected the proteins to SDS-PAGE, an anti-HA antibody revealed a strong signal with an apparent molecular weight of ~65

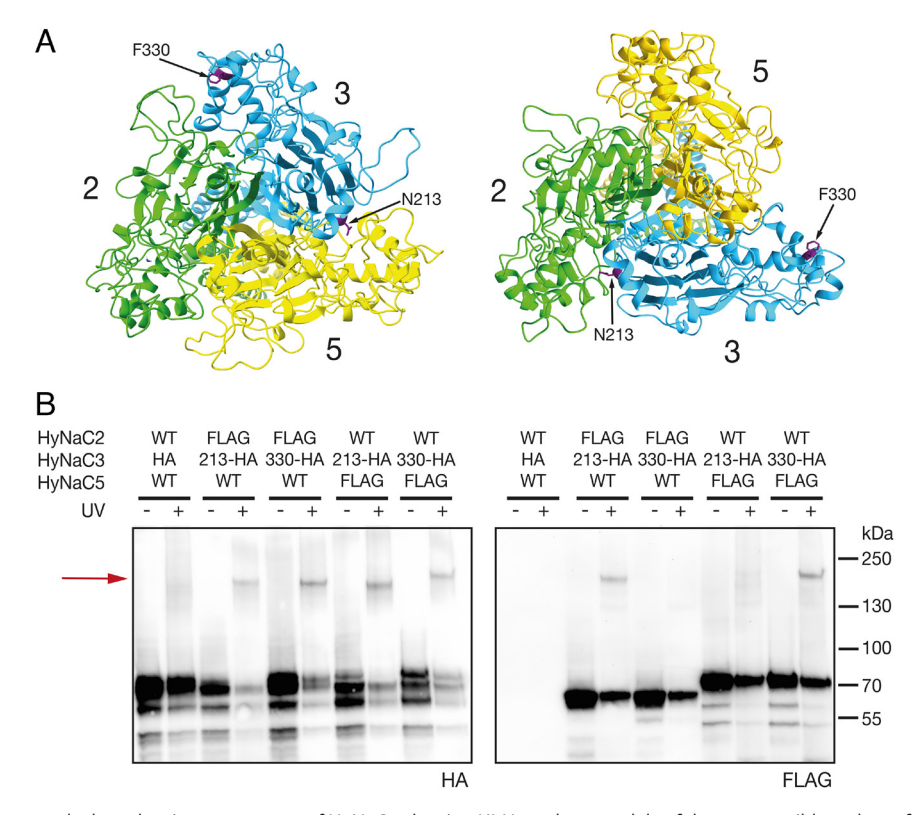


Fig. 1. Photo-cross-linking reveals the subunit arrangement of HyNaC subunits. (A) Homology models of the two possible orders of the HyNaC subunits, based on the closed conformation of cASIC1. Left, the clockwise 2-3-5 order, and Right, the clockwise 2-5-3 order, viewed from the top. HyNaC2 is depicted in green, HyNaC3 in blue, and HyNaC5 in yellow. Residues 3-N213 and 3-F330 are highlighted with purple sticks. (B) Western blot analysis illustrating cross-linking of two subunits after UV irradiation. HyNaC2, HyNaC3, and HyNaC5 were coexpressed in HEK293 cells; subunits carried HA or Flag epitopes as indicated. The red arrow indicates putative cross-linked dimeric complexes with an apparent molecular weight of ~150 kDa. On the Left, HyNaC3-containing complexes were detected with an anti-HA antibody, and on the Right, HyNaC2- or HyNaC5-containing complexes were detected on the same blot with an anti-FLAG antibody.

kDa, corresponding to a single HyNaC3 subunit. However, in cells treated with UV light, another band with a molecular weight that corresponds to a dimer was detected. This dimer was absent when cells were not treated with UV light and in cells expressing wildtype HyNaC3, showing that the dimer was only formed when UV light was applied and when azF was present, suggesting that azF at positions 213 and 330 cross-linked HyNaC3 to its neighboring subunit (Fig. 1B). To identify the subunit that was cross-linked, we probed the same western blots with an anti-Flag antibody; either HyNaC2 or HyNaC5 carried a Flag epitope. This revealed that HyNaC3 carrying an azF at position 213 was cross-linked to HyNaC2. In contrast, HyNaC3 carrying an azF at position 330 was cross-linked to HyNaC5 (Fig. 1B). Both results are consistent with a clockwise 2-5-3 arrangement of subunits when viewed from above (Fig. 1A). We found no evidence in favor of the 2-3-5 arrangement, suggesting that a channel with the 2-5-3 arrangement is the predominant (and perhaps the only) form of HyNaC2/3/5.

The HyNaC5-3 Interface Is Crucial for Activation by Hydra RFamides. We used refined homology modeling based on the crystallographic structure of cASIC1 in the open conformation (PDB ID 4NTW) to generate 200 models of HyNaC2/3/5 having

a clockwise 2-5-3 order when viewed from the top (Fig. 1A). The 10 models with the highest score (see Methods for details) were chosen for further analyses. The models predicted an overall structure for HyNaC2/3/5 that was similar to that of cASIC1 with conserved α -helices and β -sheets. Analyses of possible binding sites with the SiteMap tool (32, 33) predicted a druggable cavity at subunit interfaces at a position corresponding to the acidic pocket of ASICs (SI Appendix, Table S1 and Fig. S2). Therefore, we substituted at least six different amino acids at each of the three different interfaces (2-5, 5-3, and 3-2, respectively). We introduced initially amino acids with side chains that might interfere with putative molecular interactions with RFamides or cause steric constraints. When these substitutions altered apparent affinity for RFamide I, we introduced additional amino acids with milder chemical differences of their side chains. We coexpressed mutant subunits individually with the two other wild-type subunits in Xenopus oocytes. Then, we determined the apparent affinity to RFamide I using a two-electrode voltage clamp (TEVC), revealing that substitutions at the 2-5 and 3-2 interfaces did not affect apparent peptide affinity (Fig. 2), except for the K214E substitution in HyNaC2, which increased apparent affinity ~10-fold (from 5 μ M to 0.7 μ M; P = 0.84). In contrast, many mutations at the

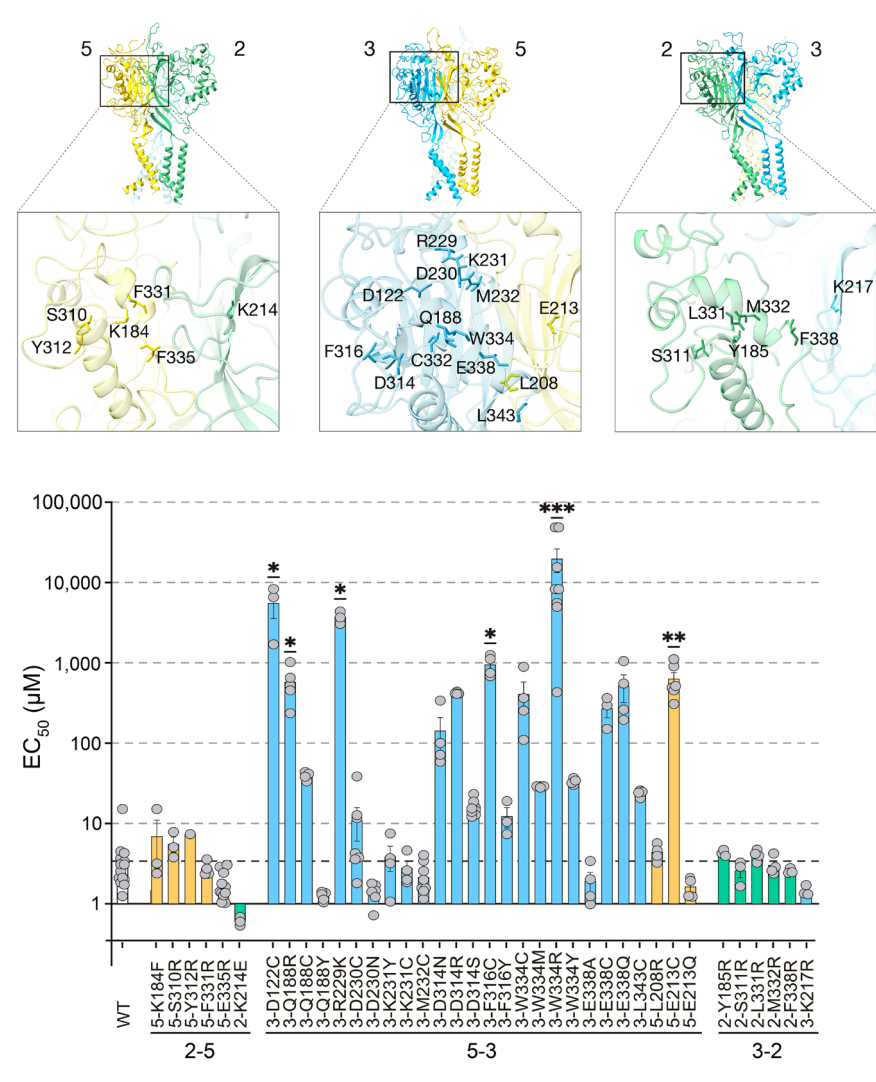


Fig. 2. Site-directed mutagenesis identifies residues at the 5-3 interface important for activation by RFamide I. Top, sideview on the three interfaces in a homology model of HyNaC2/3/5, based on the open conformation of cASIC1. The position of substituted amino acids is indicated. HyNaC2 is shown in green, HyNaC3 in blue, and HyNaC5 in yellow. Bottom, EC₅₀ values (mean ± SD) for activation by RFamide I for wild-type HyNaC2/3/5 and mutant channels. One subunit carrying the indicated mutations was coexpressed with the other two wild-type subunits. Mutants are grouped by interfaces. The dashed black line indicates the mean EC_{50} value of the wt. *P < 0.05; **P < 0.01; ***P < 0.001 (one-way ANOVA).

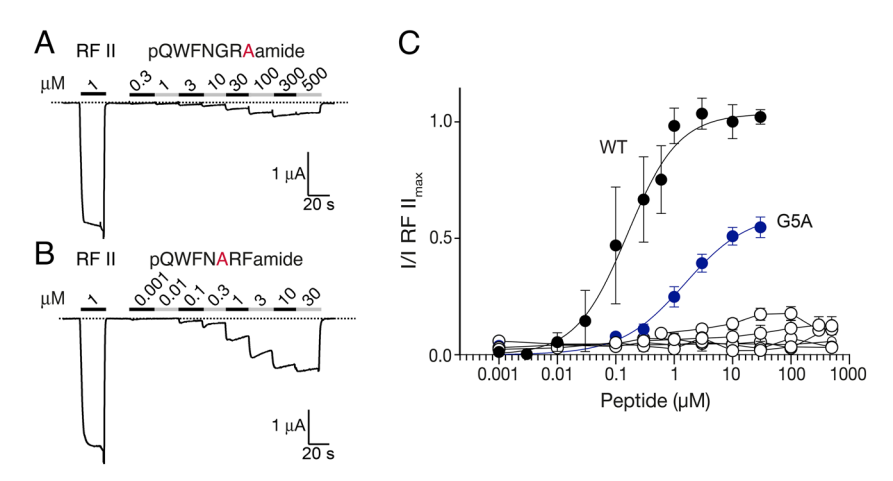


Fig. 3. Alanine scanning of RFamide II reveals residues important for activation of HyNaCs. (A) Representative current trace for activation with the F7A mutant. Wild-type RFamide II (1 μ M) was used as control. (B) As in (A), but for G5A. (C) Concentration–response relationships (mean \pm SD) for wild-type RFamide II (black circles; n = 15), G5A (blue circles; n = 5), pQ1A (n = 11), W2A (n = 10), F3A (n = 5), N4A (n = 8), R6A (n = 5), and F7A (n = 6) (open circles).

5-3 interface reduced apparent peptide affinity, some more than 2,000-fold (Fig. 2). Most mutations that reduced EC₅₀ were on HyNaC3, suggesting that HyNaC3 contributes the principal side of the ligand-binding pocket and HyNaC5 the complementary side. In particular, substitutions of 3-D122, 3-Q188, 3-R229, 3-D314, 3-W334, and 3-E338 on the principal side and of 5-E213 on the complementary side reduced sensitivity to RFamide I, highlighting that the lower finger, β -ball, and thumb domains make major contributions to peptide sensitivity. Importantly, substitutions of equivalent residues on the 3-2 and 2-5 interfaces did not affect peptide sensitivity. For example, the substitution of 3-D314 by Arg reduced EC₅₀ ~200-fold (P = 0.058), whereas substitutions of the equivalent residues 2-S311 and 5-S310 by Arg did not affect EC₅₀. Likewise, substitution of 3-W334 by Arg reduced EC₅₀ ~1,000-fold (P < 0.001), whereas substitutions of the equivalent residues 2-M332 and 5-F331 by Arg did not affect EC₅₀. These results indicate that subunit interfaces do not equally contribute to the activation of HyNaC2/3/5 by RFamide I. The strong reduction in apparent affinity suggested that RFamide I may bind to the lower finger, β-ball, and thumb domains at the 5-3 interface to activate HyNaC2/3/5.

Almost All Residues of RFamide II Are Crucial for Its Function.

To assess which residues of Hydra RFamides are important for HyNaC activation, we conducted an alanine scan of RFamide II (pQWFNGRFamide). We selected this peptide because of its 10-fold higher apparent affinity compared with RFamide I (31). We substituted each amino acid of the peptide individually with alanine and assessed EC50 values by TEVC in oocytes. Strikingly, all substitutions led to a loss of function (up to 600 µM peptide), except for the G5A substitution, but which also reduced the potency and efficacy of the peptide (EC₅₀ = 1.6 \pm $0.2 \,\mu\text{M}$ compared with $0.3 \pm 0.06 \,\mu\text{M}$, P = 0.004; Fig. 3). These results indicate that nearly all residues of RFamide II are essential for its function. However, RFamide I (pQWLGGRFamide) differs from RFamide II at positions 3 and 4, yet has an EC₅₀ of ~5 µM (31), indicating that at least at these two positions there is some structural flexibility and that the exchange of F3 by Leu and of N4 by Gly is better supported than the exchange by Ala.

A Molecular Interaction Model for RFamides and the Cavity at the 5-3 Interface. To corroborate the mutagenesis results, we used the identified cavity at the 5-3 interface in the ECD of HyNaC2/3/5 as the docking site for RFamide I and RFamide II. Each neuropeptide had 100 binding poses generated across the 10 homology models

of the channel with the highest score, resulting in 1,000 poses per neuropeptide. The resulting set of poses was filtered based on their Glide score (34) and on a Tanimoto similarity score, which represents the overlap between the interacting residues in the pose and a subset of seven HyNaC3 residues found in mutagenesis experiments (*Methods*). None of the poses could interact simultaneously with all the HyNaC residues in the reference group. Nonetheless, the selected poses showed a common binding configuration and recurrent interactions with a conserved set of residues (Fig. 4A; for a comparison with all docking results, see *SI Appendix*, Fig. S3). The best poses for both neuropeptides were found deep in the analyzed pocket, completely surrounded by HyNaC3 and HyNaC5 residues (Fig. 4 *B–D* and *SI Appendix*, Fig. S4). This is in contrast to the shallower poses observed for FMRFamides on FaNaCs (17, 18). In our models, the ligand-binding pocket is shifted closer to the membrane and core of the protein. The ligand backbone partially aligns with the channel's main axis: The C-terminal Phe residue (F7) is anchored in the 5-3 interface via π - π interactions, while the N-terminal pyroglutamate (pQ1) extends extracellularly (Fig. 4D and SI Appendix, Fig. S4). This set of selected poses also corroborates the experimental results, given that almost all the side chains of the neuropeptides play a relevant role in proper binding and recognition. The most consistent interactions between RFamides and HyNaC2/3/5 include both hydrophobic and electrostatic interactions (Fig. 4E and *SI Appendix*, Fig. S5) and were as follows: i) a π – π interaction between W2 and 5-Y154, especially maintained in the selected RFamide II poses (SI Appendix, Fig. S5); ii) H-bonds between R6 and 5-E213 and 3-E338; iii) an H-bond between the backbone carbonyl of R6 and 3-Q188; iv) a π - π interaction between F7 and 3-W186; and v) an H-bond between the backbone carbonyl of F7 and 3-K249. While these interactions are conserved for both RFamide I and RFamide II, the side chains of residues 3 and 4, which differ between the two peptides (LG in RFamide I and FN in RFamide II), did not make consistent interactions in our models, consistent with the fact that both peptides are agonists at HyNaC2/3/5, although with different potencies (~5 μM for RFamide I and ~0.4 μM for RFamide II) (31). These results identify a binding pocket that largely overlaps with the pocket identified by site-directed mutagenesis of HyNaCs. Moreover, some specific residues, for example 3-Q188, 5-E213, and 3-E338, were identified by both methods to make important contributions to peptide binding or apparent affinity.

Covalent Cross-Linking of RFamide II to HyNaC2/3/5 Confirms Its Binding to the Conserved Pocket. To obtain more direct evidence for a binding site at the 5-3 interface, we turned to photo-cross-linking employing noncanonical amino acids in living cells. This

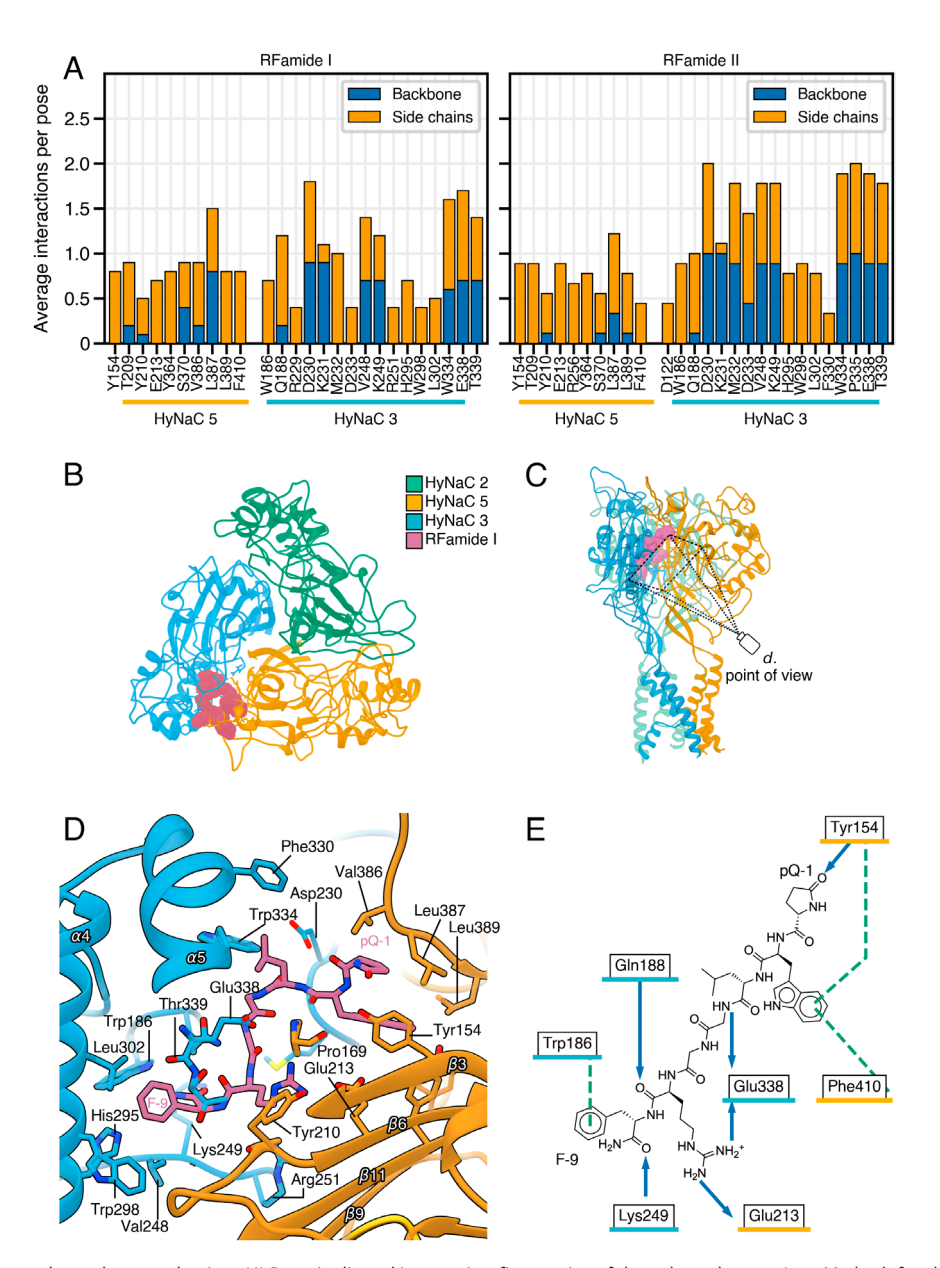


Fig. 4. Molecular docking results and pose selection. (A) Protein-ligand interaction fingerprint of the selected poses (see Methods for details) for RFamide I (Left panel) and RFamide II (Right panel). For each residue, the average number of interactions with the bound poses is reported. The bar color represents whether an interaction is formed between the ligand and the backbone (blue) or the side chain (gold) of the residue. Only bars with a value larger than 0.3 are displayed. (B) Top and (C) side view of the bound pose within the homology model. Green, yellow, and light blue ribbons and sticks represent HyNaC2, HyNaC5, and HyNaC3, respectively. The ligand is colored in reddish purple. (D) Detailed stick representation of RFamide I in the binding pocket. All residues within 3.0 Å of the neuropeptide are shown. Point of view as indicated in (C). For RFamide II, see SI Appendix, Fig. S4. (E) Schematic representation of the hydrogen bonds (blue arrows) and aromatic interactions (green dashed lines) between the top-scoring pose of the neuropeptide and the protein.

approach has previously been successfully used to confirm the Big Dyn-binding site in ASIC1a (28). We substituted 25 amino acids not only close to the suspected binding pocket at the 5-3 interface but also at the corresponding location in the other two interfaces by azF. Functional analyses in HEK293 cells revealed that 16 out of the 25 mutants were functional with current amplitudes >200 pA and were almost fully activated by 1 µM RFamide II (SI Appendix, Fig. S6). We chose positions 3-F330 and 3-E338 for further analyses because they localize to opposite sides of the putative binding pocket at the 5-3 interface and because RFamide II elicited relatively large currents with these mutants (SI Appendix, Fig. S6). HEK cells expressing 3-F330azF or 3-E338azF together with wt HyNaC2 and HyNaC5 were treated with UV light for 20 min, either in the absence or presence of 5 μM RFamide II. Then, we conducted patch-clamp recordings of these cells. We reasoned that the covalent attachment of RFamide II to its

binding site might constitutively activate the channels (Fig. 5A); therefore, to avoid damage to the cells by the constant influx of Na⁺, we kept the cells in a bath solution in which we replaced Na⁺ with the impermeant cation NMDG⁺. For cells that had been treated with UV light in the absence of the peptide, we recorded only small inward currents when we exchanged the NMDG solution with the standard bath containing Na⁺. Furthermore, the application of RFamide II to these cells elicited large currents with amplitudes of 445 ± 40 pA (3-F330azF) and 403 ± 61 pA (3-E338azF), respectively (n = 5; Fig. 5). In striking contrast, for cells that had been treated with UV light in the presence of the peptide, we recorded large inward currents (438 ± 86 pA and 387 ± 58 pA, respectively; n = 5) already upon exchanging the NMDG solution with the standard bath containing Na⁺, and the application of RFamide II did not elicit larger currents (Fig. 5). These results show that UV light in the presence of

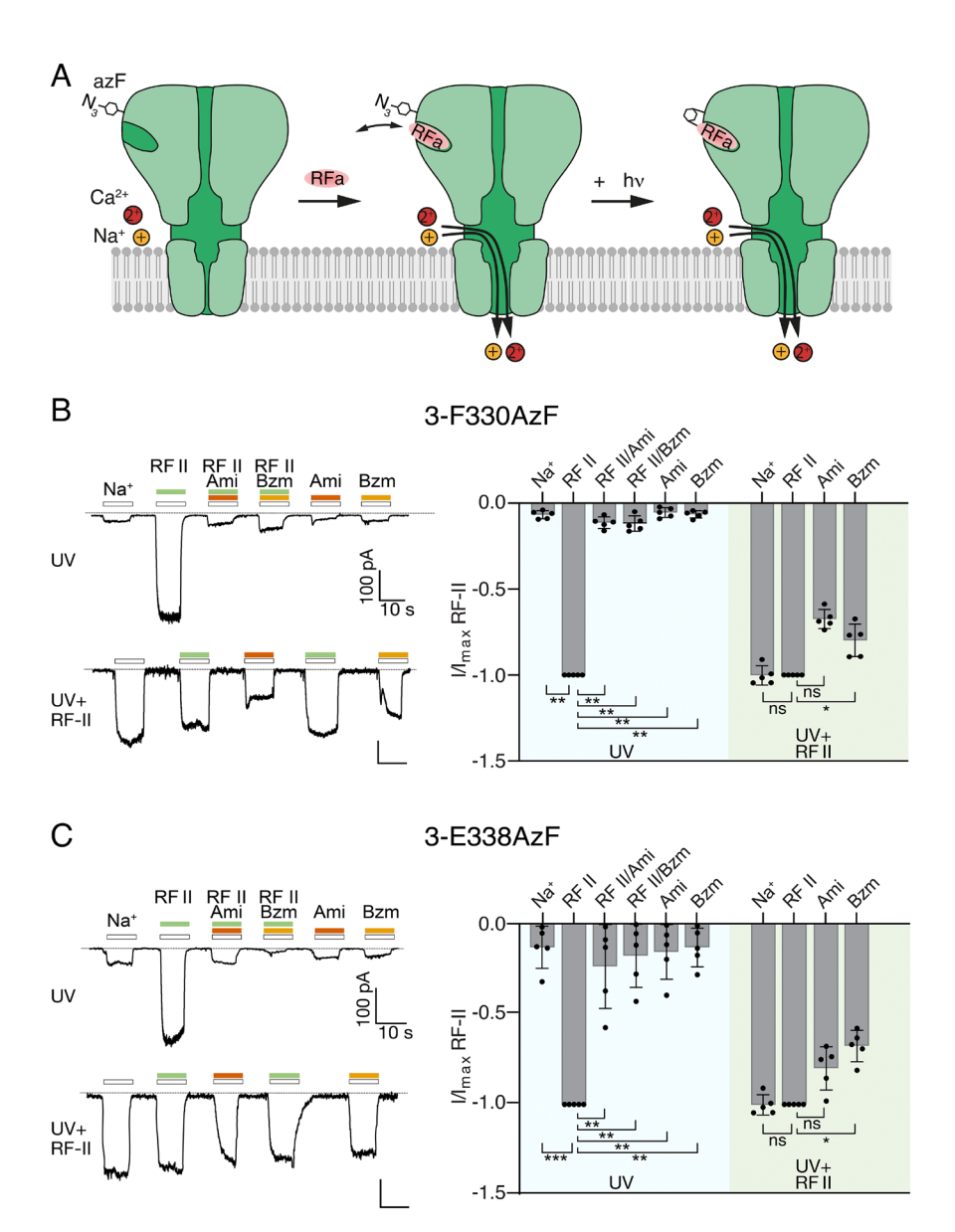


Fig. 5. Covalent cross-linking of RFamide II constitutively activates HyNaC2/3/5. (*A*) Scheme illustrating how cross-linking RFamide peptides (RFa) to HyNaC might constitutively open the ion pore. (*B*) *Left*, representative current traces for 3-F330azF coexpressed with HyNaC2/5 wild-type. *Top*, for cells that had been treated with UV light. *Bottom*, for cells that had been treated with UV light in the presence of 5 μ M RFamide II (RF II). *Right*, normalized summary data (mean \pm SD). Absolute current amplitudes (mean \pm SD) were 445 \pm 40 pA for cells treated with UV light and 438 \pm 86 pA for cells treated with UV light in the presence of RFamide II. (*C*) As in (*B*) but for 3-E338azF. Absolute current amplitudes were 403 \pm 61 pA for cells treated with UV light, and 387 \pm 58 pA for cells treated with UV light in the presence of RFamide II. **P* < 0.05; ***P* < 0.01; ****P* < 0.001 (one-way ANOVA).

RFamide II-induced constitutive Na⁺ currents in cells expressing 3-F330azF or 3-E338azF together with HyNaC2/5. Moreover, they demonstrate that tethering a single peptide ligand to the channel is sufficient for full activation. Importantly, in control cells expressing HyNaC2/3/5 wt (carrying no azF substitution), UV light did not induce constitutive currents, even when the peptide was present during UV treatment (SI Appendix, Fig. S7A), illustrating that the constitutive currents relied on the presence of azF at position 3-330 of 3-338, close to the entrance of the putative peptide-binding pocket. Moreover, the amplitude of the constitutive currents was reduced by the HyNaC pore blockers amiloride and benzamil (Fig. 5), confirming that they were indeed mediated by HyNaCs. It is noteworthy that the potency of the two blockers was lower than anticipated (31). We speculate that the conformation of the ion pore was slightly changed by the covalent attachment of the peptide ligand. To further prove the specificity of these results and for the presence of a single ligandbinding pocket at the 5-3 interface, we substituted positions 5-F327 (corresponding to 3-F330) and 5-E335 (corresponding to 3-E338), which are located at the 2-5 interface, by azF. Strikingly, UV light in the presence of RFamide II did not induce constitutive currents when these subunits were coexpressed with the other two wt subunits (*SI Appendix*, Fig. S7 *B* and *C*), providing independent proof that HyNaC2/3/5 has a single peptide-binding pocket at the 5-3 interface.

Discussion

Our study has two major findings. First, we demonstrated that the subunits of the HyNaC2/3/5 heterotrimer have a 2-5-3 order. Second, we identified a putative peptide-binding pocket in HyNaCs, which is different from that in FaNaCs but is conserved in ASICs, where it also binds peptide ligands. Site-directed mutagenesis identified a pocket in the ECD of HyNaC2/3/5, where mutations strongly reduced apparent peptide affinity. Unexpectedly, only mutations of this region at the 5-3 but not the 2-5 and 3-2 interfaces

reduced affinity, showing that the pocket at the 5-3 interface has a specific role in determining peptide affinity. While mutagenesis alone does not suffice to differentiate between an effect on the binding of peptides and on gating movements, molecular docking identified a binding pocket at the 5-3 interface that could tightly accommodate RFamide I and II and which substantially overlapped with the residues identified by mutagenesis. Strikingly, the corresponding binding pocket at the 2-5 and 3-2 interfaces failed to be consistently identified by in silico binding site searches across the homology models. Moreover, the covalent cross-linking of RFamide II to residues 3-F330 and 3-F338 at the entrance of the putative pocket constitutively activated HyNaC2/3/5. Importantly, while residue F330 is at the entrance to the pocket, E338 is within the pocket (Fig. 4D), rendering binding of the peptide to another binding site highly unlikely. Additionally, further application of RFamide II to channels with a cross-linked peptide did not increase current amplitudes, indicating that a single peptide ligand is indeed sufficient for full activation of HyNaC2/3/5. Collectively, these results strongly suggest that HyNaC2/3/5 has a single peptide-binding pocket at the 5-3 interface, in the same region as the acidic pocket of ASICs.

HyNaC subunits assemble into functional heteromeric ion channels by combining HyNaC2 with one subunit from subgroup 1 (HyNaC5, HyNaC6, or HyNaC7) and another from subgroup 2 (HyNaC3, HyNaC4, HyNaC8, HyNaC9, HyNaC10, or HyNaC11) (8). An alignment of HyNaC sequences in the critical regions—finger, β -ball, and α 5 of the thumb—reveals that these regions are much better conserved within one subgroup than between the two subgroups (Fig. 6A). Moreover, some of the residues identified by mutagenesis and docking are conserved in one group but not the other. Specifically, residues 3-Q188, 3-D230, and 3-W334 are conserved in all group 2 subunits but are absent in group 1 subunits. And residue 5-E213 is conserved in all group 1 subunits but is absent in group 2 subunits (Fig. 6A). For residues 3-R229 and 3-E338, the picture is more ambiguous. These results further confirm the importance of these residues for HyNaC activation and suggest that group 2 subunits can replace HyNaC3 and group 1 subunits HyNaC5 to form a conserved ligand-binding pocket. Interestingly, none of the key residues is conserved in HyNaC2 (Fig. 6A), explaining why this subunit can neither contribute to the principal nor the complementary ligand-binding side. Because HyNaC2 is an obligate subunit of functional

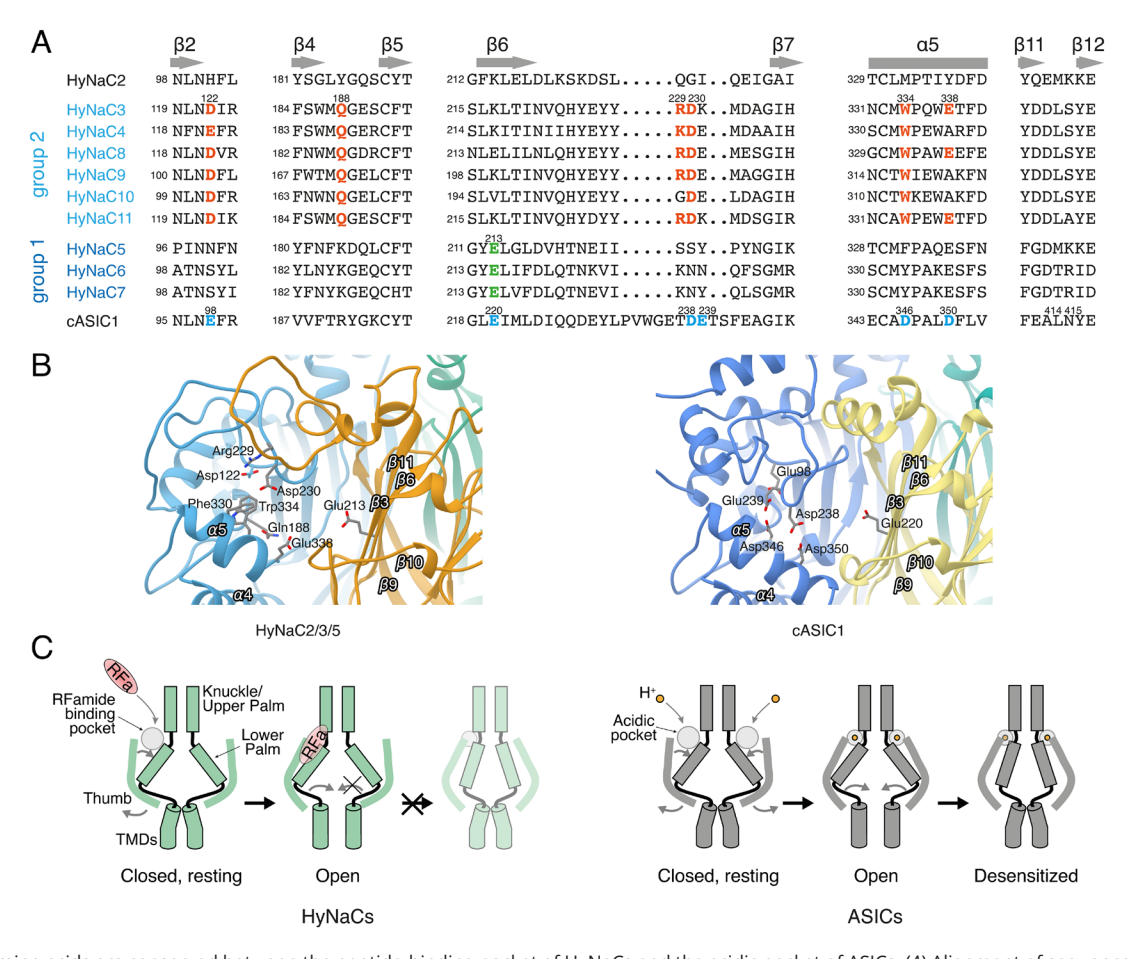


Fig. 6. Key amino acids are conserved between the peptide-binding pocket of HyNaCs and the acidic pocket of ASICs. (A) Alignment of sequences contributing to the peptide-binding site in HyNaCs with the corresponding sequence of cASIC1. The linker following $\beta 2$ is in the lower finger, $\beta 4-\beta 7$ are in the β -ball, and $\alpha 5$ is in the thumb domain. Conserved residues on the principal side of the HyNaC binding site are in bold red, those on the complementary side are in bold green, and amino acids contributing to the acidic pocket of cASIC1 are in bold blue. Note that the β6-β7 linker is shorter in HyNaCs than in cASIC1 and the alignment in this region is ambiguous. The sequences of the β11- β12 linker, which is not involved in peptide binding, are also shown. Numbers above sequences indicate positions in HyNaC3, HyNaC5, and cASIC1, respectively; positions of α -helices and β -sheets above sequences are based on cASIC1 (12). (B) View under a comparable angle into the peptide binding pocket at the 5-3 interface (Left) and into the acidic pocket of cASIC1 (Right). Amino acids highlighted in (A) are indicated. Green, yellow, and light blue subunits correspond to HyNaC2, HyNaC5, and HyNaC3, respectively; the three cASIC1a subunits are distinguished by similar colors. (C) Scheme illustrating how a single peptide binding site may be sufficient to open the HyNaC ion pore. Binding of a single RFamide could induce movement of a single thumb domain, closing the binding pocket which is transmitted to the lower ECD to open the ion pore. However, the incomplete movement of all three thumb domains might prohibit gating movements that are associated with desensitization in ASICs. In ASICs all three thumb domains move upon binding of protons, opening the ion pore and allowing concomitant desensitization.

HyNaCs (8), this feature predicts that all HyNaCs have only one ligand-binding pocket per channel. We speculate that HyNaC2 is critical for the assembly of HyNaCs.

We also compared HyNaC sequences with the cASIC1 sequence (Fig. 6 A and B). Strikingly, some of the important residues in HyNaCs have positions that correspond to those of acidic residues forming the acidic pocket (12). For example, 5-E213 occupies the equivalent position as E220 in cASIC1, and 3-W334 and 3-E338 as D346 and D350, respectively. In cASIC1, E220 interacts with D408, D346 with E239, and D350 with D238 (12). Because the residues corresponding to D408 and D346 are hydrophobic in all group 1 and 2 HyNaCs, only the pair corresponding to D350-D238 (E338-D230 in HyNaC3; Fig. 6 A and B) is conserved in three out of six group 2 HyNaCs but the loop linking β6 and β7 (which contains D238) is shorter in HyNaCs (Fig. 6A), and this pair did not interact in our homology models (Fig. 6B), suggesting that there are no carboxyl-carboxylate interactions in HyNaCs. Nevertheless, the similar positions of these amino acids as acidic residues in ASICs suggest that these positions play a pivotal role in gating across these ion channels.

We propose that upon binding Hydra RFamides, the peptide-binding pocket of HyNaCs contracts around the ligand by moving the thumb toward the β-ball domain, which triggers the opening of the HyNaC ion pore, similar to what has been suggested for ASICs (24). However, according to current knowledge, peptides are not natural ASIC agonists (35, 36), and, therefore, ASICs need a different mechanism to keep the pocket extended in the closed state and contracted in the open state. There is evidence that divalent cations (such as Ca²⁺) are coordinated by cASIC1 residues E98 and E239 at the top of the acidic pocket in the closed (expanded) state but not in the desensitized (contracted) state (37). Interestingly, E98 corresponds to residue 3-D122 of the finger domain; E239 is not conserved in HyNaC3 (Fig. 6A). These observations support the existence of an important role for finger residue 3-D122 and suggest that the ASIC binding pocket evolved into an acidic pocket, for example by additional residues in the $\beta6-\beta7$ loop, which allowed the coordination of a Ca²⁺ ion by acidic residues to keep the pocket in an extended conformation in the closed state. It has previously been proposed that upon proton binding, acidic residues within the pocket get protonated, the Ca²⁺ ions get displaced, carboxyl-carboxylate pairs form and the pocket collapses (12, 19). In this scenario, the acidic pocket plays a crucial role in ASIC gating, particularly for its modulation by divalent cations (38, 39). However, it does not exclude the possibility that protons binding at other positions trigger the opening of an ASIC, as several studies suggest (19–22).

Although no peptides directly activating ASICs are known (35, 36), some bind to the acidic pocket in either its extended or its contracted conformation. For example, the opioid neuropeptide Big Dyn binds deep into the acidic pocket of ASIC1a (27, 28) in its extended conformation, preventing its collapse and stabilizing the closed state (28). In contrast, the cystine knot toxin psalmotoxin 1 (PcTx1) from a South American tarantula docks on the thumb domain and interacts intimately with the acidic pocket in its contracted conformation (25, 26), promoting its collapse and stabilizing the open and desensitized states (29, 40). Although Big Dyn and PcTx1 are relatively large peptides (32 and 40 amino acids, respectively) and make many specific interactions with the acidic pocket, there are some recurring key interactions with residues corresponding to HyNaC residues involved in binding Hydra RFamides (Fig. 6A). These key interactions include those with E98 of the finger, E220 of the β-ball, and D346 and D350 of the thumb (25–28). Thus, some residues making key interactions with neuropeptide ligands are conserved across ASICs and HyNaCs (Fig. 6A) and have also been exploited by venomous animals to target ASICs. Furthermore, high-affinity small-molecule inhibitors of ASIC1 exploit some of the same interactions (41, 42). These findings further underscore the importance of these residues for ligand binding in a conserved pocket of clade A DEG/ENaCs.

What happens during channel opening to the two interfaces of a HyNaC that include HyNaC2 residues and do not bind peptides? Will their thumb also move toward the β-ball domain? The answer to this question may be linked to a unique property of HyNaCs: lack of desensitization. Desensitization is a hallmark of ligand-gated ion channels, including FaNaC and ASICs. However, HyNaCs do not desensitize, even in the prolonged presence of the ligand (8, 43) and this property may be important for their physiological functions in epitheliomuscular cells of Hydra (44). Desensitization of ASICs is mediated by a molecular clutch that uncouples the upper ECD from the lower ECD and ion pore, such that the ion pore closes even with a contracted acidic pocket (24) (Fig. 6C). If only the thumb at the 5-3 interfaces moved toward the β-ball domain, it might be that the lower ECD of HyNaCs cannot uncouple from the upper ECD, essentially preventing desensitization (Fig. 6C). In this scenario, the sustained opening of HyNaCs in the presence of a ligand is a consequence of it having a single peptide-binding site. In support of this scenario, it has been shown that kainate-type ionotropic glutamate receptors that are not fully occupied by ligands can open without desensitization (45). Interestingly, amino acids of the β 11– β 12 linker that constitutes the molecular clutch of ASICs and which undergoes a simple rearrangement to permit rapid desensitization (24) are well conserved within group 2 HyNaCs and similar to the β11-β12 linker of cASIC1 (Fig. 6A). L414 and N415 of cASIC1 are of particular importance for desensitization (46) and L414 is completely conserved and N415 is replaced by a serine or an alanine in group 2 HyNaCs. In contrast, L414 is not conserved and N415 is replaced by a bulky, positively charged residue (Arg or Lys) in group 1 HyNaCs and HyNaC2 (Fig. 6A). These observations suggest that only the group 2 subunit in a heterotrimeric HyNaC, which also contributes the principal side of the peptide binding pocket, has a molecular clutch similar to ASICs, further suggesting that structural elements of the other two subunits may prohibit desensitization. However, other residues also influence desensitization of ASICs (47–49), and further experiments are necessary to address the molecular basis of the lack of desensitization in HyNaCs.

Our study has certain limitations. In silico docking was based on homology models that may not faithfully represent the structure of the channel. Therefore, while the binding poses of RFamide I and RFamide II proposed similar key interactions between ligands and receptor, molecular interactions of specific amino acids need to be interpreted with care. In addition, there was not a perfect match between amino acids identified by molecular docking and mutations that reduced apparent peptide affinity. Nevertheless, site-directed mutagenesis and sequence comparisons with other HyNaCs and cASIC support the importance of several amino acids identified by our models to make important contributions to ligand binding. Another limitation is that we analyzed HyNaC mutants for the apparent affinity of RFamide I and that we performed an alanine scan and covalent cross-linking of RFamide II. Based on the evolutionary relation of the two ligands and their conserved sequence with five out of seven identical residues, we believe we can assume that both ligands have the same binding site, where they make conserved interactions.

In summary, our study establishes a 2-5-3 order of HyNaC subunits and strongly suggests the presence of a single peptide-binding site at the 5-3 interface. While the details of peptide-channel interactions have to be interpreted with care, we identified several key positions within this pocket that are conserved across HyNaCs and ASICs and appear to be pivotal for ligand binding in clade A DEG/ ENaCs.

Methods

Peptide Synthesis and Handling. Peptides were purchased from ProteoGenix (Schiltigheim, France) with a purity of >83 %. Depending on their properties, they were reconstituted in a 3:1 or 2:1 mixture of deionized water:DMSO at concentrations of 1.6 to 50 mM. For electrophysiological and biochemical analyses, the peptides were diluted to their final concentrations, either in standard bath solution, Hank's Balanced Salt Solution (HBSS), or phosphate-buffered saline (PBS). Experimental solutions were freshly prepared before their use.

Functional Expression in Xenopus Oocytes. Stage V-VI oocytes were collected from anesthetized Xenopus laevis adult females (2.5 g/L tricainemethanesulfonate for 20 to 30 min). Anesthetized frogs were killed after the final oocyte harvest by decapitation. Animal care, surgery, and experiments were performed in accordance with the German Law on the protection of animals and were approved by the ministry for environment, nature and consumer protection (LANUV) of the State North Rhine-Westphalia (NRW) under number 81-02.04.2019.A356.

cRNA for HyNaC2, HyNaC3, and HyNac5 was synthesized from linearized cDNA using the mMessage mMachine SP6 kit (Thermo Fisher Scientific, Grand Island, NY) and purified with RNA Clean & Concentrator-TM-25 (Zymo Research Europe GmbH, Freiburg, Germany). RNA concentrations were determined at 260 nm, and quality was confirmed on a 1% agarose gel. The cRNA concentration was adjusted to \sim 200 ng/ μ L, and aliquots were stored at -80 °C. Approximately 1.6 ng cRNA of a 1:1:1 mixture of the three subunits was injected into defolliculated oocytes, and oocytes were incubated at 19 °C for 2 d in OR-2 solution containing (in mM): 85 NaCl, 2.5 KCl, 1 Na₂HPO₄, 1 MgCl₂, 1 CaCl₂, 5 HEPES, 0.5 g/L PVP, 1,000 U/L penicillin, and 10 mg/L streptomycin; pH was adjusted to 7.4 using NaOH.

TEVC experiments were performed using a Turbo Tec-03X amplifier (npi electronic GmbH, Tamm, Germany), and data were recorded with CellWorks 6.2.1 (npi electronic GmbH) at 1 kHz. Glass electrodes filled with KCl (0.3 to 1.5 M Ω resistance) were employed with a holding potential of -70 mV throughout the recordings. Fast solution exchange was facilitated by the programmable pipetting robot ScreeningTool (npi electronic GmbH).

The standard bath solution contained (in mM): 140 NaCl, 10 HEPES, 1.8 CaCl₂, and 1 MgCl₂; pH was adjusted to 7.4 using NaOH. Peptide stocks were added to the bath solution just before each experiment to achieve the desired working concentration. Due to the Ca²⁺ permeability of HyNaCs (43), oocytes were injected with 50 nL of 20 mM EGTA before measurements to avoid activation of endogenous Ca²⁺-activated Cl⁻ channels (CaCCs). Oocytes from at least two frogs were used in the experiments.

Homology Model Generation and Peptide Docking. The sequences of HyNaC2, HyNaC3, and HyNaC5 were retrieved from Uniprot (IDs: A8DZR6, D3UD58, and A8DZR7). A blast search in the Protein Data Bank database revealed that the best template to model the trimeric protein in the open state was ASIC1 of the species Gallus gallus, with PDB ID 4NTW. To enhance the alignment quality between the sequence to be modeled and the template, we incorporated the biological information from the two taxonomic groups. Namely, the alignment with clustalW was repeated by including the 1,750 most similar sequences belonging to the Hydroidolina (taxid: 37516) and Aves groups (taxis: 8782). These sequences were obtained from the database of nonredundant protein sequences via blastp. The process was repeated for every monomer and the alignment to the ASIC structure sequence was used as input in Modeller 9.25 to generate 200 models scored with the DOPE-HR metric. The models were additionally evaluated with Procheck 3.5.4 and ranked by the product of their procheck and DOPE-HR score.

The ten best models were imported in Maestro version 12.6.144 (Schrödinger Release 2020-4: Maestro, Schrödinger, LLC) and prepared using the default settings in the Protein Preparation Wizard menu. The structures were analyzed using SiteMap and, in all the models, a pocket was found at the interface of HyNaC5 and HyNaC3 (SI Appendix, Table S1 and Fig. S2), which was used to build a receptor grid for peptide docking. The three-dimensional structures of RFamide I and II were built in UCSF Chimera 1.14 and prepared for docking using LigPrep (Schrödinger Release 2020-4: LigPrep, Schrödinger, LLC). The Bioluminate Peptide Docking module was used to return 100 docking poses

per each ligand, per each receptor. The interactions between each pose and the receptor were analyzed using the Interaction Fingerprint tool in Maestro. For each pose and each residue, the presence and type of the interaction (backbone, side chain, polar, hydrophobic, hydrogen bond acceptor or donor, aromatic, and charged) were saved in a tabular format.

The interaction fingerprint of each ligand was compared to a binary vector representing the only theoretical case where the ligand forms, at the same time, all possible interactions with a set of selected residues, based on the experimental results and consisting of HyNaC3 residues 122, 188, 229, 314, 316, 334, and 338. The agreement between this theoretical fingerprint and one of the poses was quantified with a Tanimoto similarity score. Poses with a Glide docking score <-10.0 and Tanimoto similarity >10 % were selected for further analysis. In particular, within the selection, the same configuration was present in the three best scoring poses for both RFamide I and II, and thus, it was selected as main hypothesis and discussed in depth in the Results section.

The protein and docking results were visualized with Maestro and rendered with UCSF Chimera 1.14. The interaction fingerprints were analyzed with Python 3.9.7 and pandas 1.3.2 and visualized with matplotlib 3.4.3.

Protein Expression in HEK293 Cells and UV Cross-Linking Experiments. HEK293 T cells were cultured in Dulbecco's Modified Eagle's Medium (DMEM) supplemented with 10 % fetal bovine serum and 2 mM L-glutamine, and maintained at 37 °C in a humidified atmosphere with 5 % CO₂. The cells were grown as an adherent monolayer and passaged every 2 to 3 d; they were replaced after ~30 passages.

For expression in HEK293 cells, codon-optimized HyNaC constructs were used (50). HyNaC subunits carried a TAG stop codon at the position, where an unnatural amino acid should be placed. To introduce p-azido-L-phenylalanine (azF) into HyNaC subunits in HEK293 cells, the pIRE4-Azi plasmid from Iris Biotech GmbH was utilized. This plasmid contains four copies of a tRNA essential for bypassing stop codons, along with an azF-specific aminoacyl-tRNA synthetase. A 0.5 M stock solution of azF in 0.5 M NaOH was diluted to a working concentration of 0.5 mM in DMEM and added to the cell culture 1 h before transfection. Photo-crosslinking experiments were conducted 36 to 48 h after transfection using a homemade UV lamp (equipped with six Philips Actinic BITL 8 W bulbs) for 20 min. For optimal cross-linking efficiency, cells were at a distance < 3 cm to the UV source.

For biochemical determination of the subunit stoichiometry, HEK cells were maintained in 10 cm dishes with up to 50 % confluency and transfected with a total of 10 μg DNA (2 μg of a 1:1:1 mixture of the three HyNaC subunits and 8 μg pIRE4-Azi) mixed with 30 µg polyethylenimine (PEI). For assessing azF incorporation efficiency, the GFP stop codon mutant Y40* was cotransfected with HyNaC constructs. Twenty-four hours after transfection, the medium in 10 cm dishes was replaced with fresh DMEM containing 0.5 mM azF. For the experiment, cells were washed with cold PBS, resuspended in PBS containing 5 μ M RFamide-II, and exposed to UV light for 20 min. Cells were then resuspended in 500 μL of ice-cold lysis buffer (50 mM HEPES pH 7.5, 150 mM NaCl, 10 % glycerol, 1% Triton X-100, 1.5 mM MgCl₂, 1 mM EGTA, 1 mM DTT, and 1X Protease Inhibitor Roche, Germany) for further analysis.

For patch clamp analysis, HEK cells were maintained in 35 mm dishes and transfected with 0.5 μg each of HyNaC2, HyNaC3, and HyNaC5, 1.2 μg pIRE4-Azi, 0.3 µg GFP mutant, and 6 µL PEI. After transfection, cells were transferred to poly-D-lysine-coated coverslips in six-well plates and provided with DMEM containing 0.5 mM azF. Coverslips were washed with PBS, followed by the addition of 2 mL of a cold, Na⁺-free solution containing (in mM): 128 N-Methyl-D-Glucamine (NMDG), 5.4 KCl, 1 MgCl₂, 2 CaCl₂, 10 HEPES, and 5.5 glucose; depending on the experimental condition, 5 µM RFamide-II was added. After UV exposure for 20 min, cells were washed with PBS and cultured in fresh DMEM for recovery and subsequent patch-clamp recording.

Gel Electrophoresis and Western Blotting. Approximately 36 to 48 h after transfection, HEK 293 cells from 35 mm dishes transfected as above were washed twice with ice-cold PBS (pH 7.4), exposed for 20 min to UV light while on ice in PBS, scraped from the dishes and centrifuged (4 °C, 5 min, 1,000 rpm). After discarding the supernatant, 500 µL HEPES lysis buffer was used to lyse the cells on ice for 1 to 1.5 h with intermittent vortexing. Samples were centrifuged (4 °C, 10 min, 13,000 rpm) and the supernatant diluted in 5X sample buffer (250 mM Tris-HCl pH 6.8, 10 % SDS, 0.05 % bromphenol blue, 50 % glycerol, and 500 mM DTT). After boiling (95 °C, 7 min), 40 μL of each sample was loaded onto a 10% polyacrylamide SDS-PAGE gel and run for 1.5 to 2 h at 130 V in running buffer (25 mM Trisma Base, 200 mM glycine, and 0.1 % SDS). Next, proteins were blotted onto a PVDF membrane (ThermoFisher, Massachusetts) for 1 h at 85 V in transfer buffer (25 mM Trisma Base, 200 mM glycine, 20 % methanol), followed by 30 min incubation in blocking buffer (137 mM NaCl, 2.7 mM KCl, 25 mM Tris, pH 7.4, 0.1 % Tween®-20, and 5 % milk powder) and 30 to 120 min incubation in blocking buffer with anti-FLAG (M2, mouse monoclonal, Sigma-Aldrich, Missouri). Blots were then washed 3 × 10 min in TBS-T (137 mM NaCl, 2.7 mM KCl, 25 mM Tris, pH 7.4, and 0.1 % Tween®-20), after which a secondary antibody (HRP AP16072 goat anti-mouse polyclonal, ThermoFisher, Massachusetts) in TBS-T was added. Finally, the blot was washed 3×10 min in TBS-T and results were analyzed by adding Clarity Western ECL substrate (BioRad, California). Blots were imaged in a Chemi-Smart 5000 Image station (Vilber Lourmat, Eberhardzell, Germany). Afterward, the blot was exposed to a sequence of i) stripping buffer (200 mM glycine, 0.1 % SDS, and 0.1 % Tween®-20, pH 2.2) for 2 × 10 min, ii) PBS for 2×10 min, and iii) TBS-T for 2×5 min. This was followed by the same procedure as above starting with blocking buffer to analyze signal from an anti-HA antibody (3F10, rat monoclonal, Sigma-Aldrich, Missouri) and a secondary antibody (HRP A136P goat anti-rat polyclonal, Merck, Darmstadt, Germany).

Patch-Clamp Experiments. Approximately 48 h after transfection, and after the UV treatment, the coverslip with attached cells was mounted on the stage of an inverted phase-contrast microscope (IX71, Olympus). The recording chamber was perfused with the following bath solution (in mM): NaCl 128, KCl 5.4, HEPES 10, glucose 5.5, MgCl₂ 1, and CaCl₂ 2; pH was adjusted with NaOH to 7.4 at RT (22 to 25 °C). Patch-clamp experiments were performed in the whole-cell configuration, using an Axon-200B amplifier (Molecular Devices; San Jose, CA) and an Axon Digidata 1440 A acquisition system controlled by the Clampex 10.0 software (Molecular Devices). Signals were low pass filtered at 1 kHz and digitized at 4 kHz. Micropipettes (4 to 6 M Ω) were prepared from borosilicate glass capillaries with a micropipette puller (DMZ-Universal Electrode Puller; Zeitz Instruments, Martinsried, Germany) and filled with an intracellular solution containing (in mM): NaCl 10, KCl 121, HEPES 10, EGTA 5, and MgCl₂ 2. Holding potential was −70 mV. Capacitance and series resistances were compensated electronically at 80 %, and digital data were stored in a compatible PC for off-line analysis using Clampfit 10.0 software (Molecular Devices).

Statistical Analysis. HEK cells and oocytes were randomly assigned to experimental groups without blinding of the experimenter. For electrophysiological experiments, we used cells from a minimum of two independent transfections or at least two batches of oocytes isolated on different days from distinct animals.

- M. B. Goodman, E. M. Schwarz, Transducing touch in Caenorhabditis elegans. Annu. Rev. Physiol. 65, 429-452 (2003).
- L. Wichmann, M. Althaus, Evolution of epithelial sodium channels: Current concepts and hypotheses. Am. J. Physiol. Regul. Integr. Comp. Physiol. 319, R387-R400 (2020).
- J. Marti-Solans, A. Borve, P. Bump, A. Hejnol, T. Lynagh, Peripheral and central employment of acidsensing ion channels during early bilaterian evolution. eLife 12, e81613 (2023).
- E. Lingueglia, G. Champigny, M. Lazdunski, P. Barbry, Cloning of the amiloride-sensitive FMRFamide peptide-gated sodium channel. Nature 378, 730-733 (1995).
- A. Schmidt et al., Dual signaling of Wamide myoinhibitory peptides through a peptide-gated channel and a GPCR in Platynereis. FASEB J. 32, 5338-5349 (2018), 10.1096/fj.201800274R,
- M. Dandamudi, H. Hausen, T. Lynagh, Comparative analysis defines a broader FMRFamide-gated sodium channel family and determinants of neuropeptide sensitivity. J. Biol. Chem. 298, 102086 (2022).
- A. Golubovic et al., A peptide-gated ion channel from the freshwater polyp Hydra. J. Biol. Chem. **282**, 35098-35103 (2007).
- M. Assmann, A. Kuhn, S. Dürrnagel, T. W. Holstein, S. Gründer, The comprehensive analysis of DEG/ ENaC subunits in Hydra reveals a large variety of peptide-gated channels, potentially involved in neuromuscular transmission. BMC Biol. 12, 84 (2014).
- J. M. Aguilar-Camacho et al., Functional analysis in a model sea anemone reveals phylogenetic complexity and a role in cnidocyte discharge of DEG/ENaC ion channels. Commun. Biol. 6, 17 (2023).
- W. Elkhatib et al., Function and phylogeny support the independent evolution of an ASIC-like Deg/ ENaC channel in the Placozoa. Commun. Biol. 6, 951 (2023).
- S. Gründer, A. O. Ramírez, G. Jékely, Neuropeptides and degenerin/epithelial Na(+) channels: A relationship from mammals to cnidarians. J. Physiol. 601, 1583-1595 (2023).
- J. Jasti, H. Furukawa, E. B. Gonzales, E. Gouaux, Structure of acid-sensing ion channel 1 at 1.9 A resolution and low pH. Nature 449, 316-323 (2007).
- Y. Y. Niu et al., Exploration of the peptide recognition of an amiloride-sensitive FMRFamide peptidegated sodium channel. J. Biol. Chem. 291, 7571-7582 (2016).

Photo-cross-linking experiments were conducted with cells from two independent transfections. Each cell and oocyte served as a biological replicate for electrophysiology, while 10 cm dishes of cells were considered biological replicates for cross-linking studies.

Electrophysiological data were analyzed offline, and current amplitudes were assessed using CellWorks Reader 6.2.2 (npi electronic GmbH, Tamm, Germany) for TEVC data and ClampFit 10.0 (pClamp 10.0, Molecular Devices, Sunnyvale, CA) for patch clamp data, calculating current density by dividing maximal current amplitude (pA) by cell capacitance (pF). Data analysis was conducted using Excel (Microsoft) or Prism (GraphPad).

Dose-response curves from TEVC and patch clamp experiments were plotted as normalized current (I/I_{max}) against peptide concentration. The half-maximal effective concentration (EC_{50}) was estimated by fitting the dose-response curves in Prism using the following equation:

$$I = \frac{\left[\text{peptide}\right]^{n_{\text{Hill}}}}{\left[\text{peptide}\right]^{n_{\text{Hill}}} + EC_{50}^{n_{\text{Hill}}}},$$

where I is the normalized current (I/I_{max}), [peptide] the peptide concentration, EC_{50} the peptide concentration required for the half-maximal effect, and n_{Hill} the Hill coefficient. Data are presented as mean \pm SD, and statistical significance was determined using two-tailed t tests or one-way ANOVA in Prism 10.0 (GraphPad, San Diego, CA) with a significance threshold set at P = 0.05.

Data, Materials, and Software Availability. Datasets generated and analyzed during this study are included in this published article. The computational data have been deposited in the public repository Zenodo (51) and are accessible via the following DOI: https://doi.org/10.5281/zenodo.10926670.

ACKNOWLEDGMENTS. This work was supported by a grant of the Deutsche Forschungsgemeinschaft (GR1771/8-1) to S.G. The plasmid for the incorporation of p-azido-L-phenylalanine in mammalian systems (pIRE4-Azi) was generously provided by Irene Coin (University of Leipzig). We thank Adrienne Oslender-Bujotzek for excellent technical assistance and Lilia Leisle for advice on work with noncanonical amino acids.

Author affiliations: aMedical Faculty, Institute of Physiology, Rheinisch-Westfälische Technische Hochschule Aachen University, 52074 Aachen, Germany; bComputational Biomedicine—Institute for Advanced Simulation/Institute of Neuroscience and Medicine, Forschungszentrum Jülich, 52425 Jülich, Germany; ⁹Jülich Supercomputing Center, Forschungszentrum Jülich, 52425 Jülich, Germany; and ^dDepartment of Neurology, Rheinisch-Westfälische Technische Hochschule Aachen University, 52074 Aachen, Germany

- 14. G. A. Cottrell, M. C. Jeziorski, K. A. Green, Location of a ligand recognition site of FMRFamide-gated Na(+) channels. FEBS Lett. 489, 71-74 (2001).
- G. A. Cottrell, Domain near TM1 influences agonist and antagonist responses of peptide-gated Na+ channels. Pflugers Arch. 450, 168-177 (2005).
- Y. Furukawa, I. Tagashira, Aromatic amino acids in the finger domain of the FMRFamide-gated Na[Formula: see text] channel are involved in the FMRFamide recognition and the activation. Pflugers Arch. 475, 975-993 (2023).
- 17. F. Liu et al., Structure and mechanism of a neuropeptide-activated channel in the ENaC/DEG superfamily. Nat. Chem. Biol. 19, 1276-1285 (2023).
- 18. V. Kalienkova, M. Dandamudi, C. Paulino, T. Lynagh, Structural basis for excitatory neuropeptide signaling. *Nat. Struct. Mol. Biol.* **31**, 717-726 (2024), 10.1038/s41594-023-01198-y.

 19. M. Paukert, X. Chen, G. Polleichtner, H. Schindelin, S. Gründer, Candidate amino acids involved in
- H+ gating of acid-sensing ion channel 1a. J. Biol. Chem. 283, 572-581 (2008).
- 20. A. J. Krauson, A. C. Rued, M. D. Carattino, Independent contribution of extracellular proton binding sites to ASIC1a activation. J. Biol. Chem. 288, 34375-34383 (2013).
- $S. \, Vullo\, \textit{et\,al.}, Conformational\, dynamics\, and\, role\, of\, the\, acidic\, pocket\, in\, ASIC\, pH-dependent\, gating$ Proc. Natl. Acad. Sci. U.S.A. 114, 3768-3773 (2017).
- M. L. Rook, T. W. McCullock, T. Couch, J. D. Lueck, D. M. MacLean, Photomodulation of the ASIC1a acidic pocket destabilizes the open state. Protein Sci. 32, e4800 (2023).
- M. L. Rook, M. Musgaard, D. M. MacLean, Coupling structure with function in acid-sensing ion channels: Challenges in pursuit of proton sensors. J. Physiol. 599, 417-430 (2021).
- 24. N. Yoder, C. Yoshioka, E. Gouaux, Gating mechanisms of acid-sensing ion channels. Nature 555,
- I. Baconguis, E. Gouaux, Structural plasticity and dynamic selectivity of acid-sensing ion channelspider toxin complexes. Nature 489, 400-405 (2012).
- R. J. Dawson et al., Structure of the acid-sensing ion channel 1 in complex with the gating modifier Psalmotoxin 1. Nat. Commun. 3, 936 (2012).
- C. B. Borg et al., Mechanism and site of action of big dynorphin on ASIC1a. Proc. Natl. Acad. Sci. U.S.A. 117, 7447-7454 (2020).

- L. Leisle et al., Dynorphin neuropeptides decrease apparent proton affinity of ASIC1a by occluding the acidic pocket. J. Med. Chem. 64, 13299-13311 (2021).
- X. Chen, H. Kalbacher, S. Gründer, The tarantula toxin psalmotoxin 1 inhibits acid-sensing ion channel (ASIC) 1a by increasing its apparent H+ affinity. J. Gen. Physiol. 126, 71-79 (2005)
- T. W. Sherwood, C. C. Askwith, Dynorphin opioid peptides enhance acid-sensing ion channel 1a activity and acidosis-induced neuronal death. J. Neurosci. 29, 14371-14380 (2009).
- S. Dürrnagel *et al.*, Three homologous subunits form a high affinity peptide-gated ion channel in Hydra. *J. Biol. Chem.* **285**, 11958–11965 (2010).
- T. Halgren, New method for fast and accurate binding-site identification and analysis. *Chem. Biol.* Drug Des. 69, 146-148 (2007).
- T. A. Halgren, Identifying and characterizing binding sites and assessing druggability. J. Chem. Inf. Model. 49, 377-389 (2009).
- T. A. Halgren et al., Glide: A new approach for rapid, accurate docking and scoring. 2. Enrichment factors in database screening. J. Med. Chem. 47, 1750-1759 (2004).
- A. Vyvers, A. Schmidt, D. Wiemuth, S. Gründer, Screening of 109 neuropeptides on ASICs reveals no direct agonists and dynorphin A, YFMRFamide and endomorphin-1 as modulators. Sci. Rep.-Uk 8, 18000 (2018).
- S. Kuspiel, D. Wiemuth, S. Grunder, The neuropeptide nocistatin is not a direct agonist of acidsensing ion channel 1a (ASIC1a). Biomolecules 11, 571 (2021).
- N. Yoder, E. Gouaux, Divalent cation and chloride ion sites of chicken acid sensing ion channel 1a elucidated by X-ray crystallography. *PLoS ONE* **13**, e0202134 (2018). E. Babini, M. Paukert, H. S. Geisler, S. Gründer, Alternative splicing and interaction with dia and
- polyvalent cations control the dynamic range of acid-sensing ion channel 1 (ASIC1). J. Biol. Chem. **277**, 41597-41603 (2002).
- D. C. Immke, E. W. McCleskey, Protons open acid-sensing ion channels by catalyzing relief of Ca(2+) blockade. Neuron 37, 75-84 (2003).

- 40. P. Escoubas et al., Isolation of a tarantula toxin specific for a class of proton-gated Na+ channels J. Biol. Chem. 275, 25116-25121 (2000).
- 41. A. Buta et al., Novel potent orthosteric antagonist of ASIC1a prevents NMDAR-dependent LTP induction. J. Med. Chem. 58, 4449-4461 (2015).
- Y. Liu et al., Molecular mechanism and structural basis of small-molecule modulation of the gating of acid-sensing ion channel 1. Commun. Biol. 4, 174 (2021).
- S. Dürrnagel, B. H. Falkenburger, S. Gründer, High Ca(2+) permeability of a peptide-gated DEG/ENaC from Hydra. *J. Gen. Physiol.* **140**, 391-402 (2012).
 S. Gründer, M. Assmann, Peptide-gated ion channels and the simple nervous system of Hydra.
- J. Exp. Biol. 218, 551-561 (2015).
- A. Reiner, E. Y. Isacoff, Tethered ligands reveal glutamate receptor desensitization depends on subunit occupancy. *Nat. Chem. Biol.* **10**, 273-280 (2014).
- M. L. Rook, A. Williamson, J. D. Lueck, M. Musgaard, D. M. Maclean, beta11-12 linker isomerization governs acid-sensing ion channel desensitization and recovery. eLife 9, e51111
- A. Springauf, P. Bresenitz, S. Gründer, The interaction between two extracellular linker regions controls sustained opening of acid-sensing ion channel 1. J. Biol. Chem. 286, 24374-24384
- S. Roy et al., Molecular determinants of desensitization in an ENaC/degenerin channel. FASEB J. 27, 5034-5045 (2013).
- Y. Wu, Z. Chen, C. M. Canessa, A valve-like mechanism controls desensitization of functional
- mammalian isoforms of acid-sensing ion channels. *eLife* **8**, e45851 (2019).

 M. Bachmann, A. Ortega-Ramirez, L. Leisle, S. Gründer, Efficient expression of a cnidarian peptidegated ion channel in mammalian cells. *Channels* (*Austin*) **15**, 273–283 (2021).
- S. Albani, G. Rossetti, Data from "A conserved peptide binding pocket in HyNaC/ASIC ion channels." Zenodo. https://doi.org/10.5281/zenodo.10926670. Deposited 4 April 2024.